ELSEVIER

Journal of Photochemistry and Photobiology A: Chemistry 105 (1997) 165–181

Journal of PHOTOCHEMISTRY AND PHOTOBIOLOGY A:CHEMISTRY

Numerical self-consistent reaction field study of intramolecular charge transfer in *p*-(dimethylamino)-benzonitrile

Peter Gedeck [1], Siegfried Schneider *

Institut für Physikalische Chemie I, Universität Erlangen-Nürnberg, Egerlandstraße 3, D-91058 Erlangen, Germany

Received 15 July 1996; accepted 13 November 1996

Abstract

The numerical self-consistent reaction field (SCRF) implementation of the semiempirical program package VAMP 5.5 allows to include the solute–solvent interaction in the iterative solution of the Hartree–Fock equations. In going beyond the widely applied Onsager model, the solvent cavity is thereby approximated by a polyhedral, carrying a charge density proportional to the gradient of the molecular potential at the cavity surface due to the charge distribution in the solute molecule. The method was modified to allow the calculation of absorption and emission spectra using a nonequilibrium description of solvation. With this approach, the free enthalpy of solvation can easily be divided into the contribution originating from ultrafast electronic polarisation and from slower orientational relaxation. The newly developed program was applied to the problem of dual fluorescence of *p*-(dimethylamino)-benzonitrile (*p*-DMABN). It was found that planarisation of the amino group leads to a stabilisation of the polar excited state independently of the assumed torsional angle ϑ. In solvents, that are more polar than diethylether ($\epsilon = 4.335$), rotation of the planar dimethylamino group connected with the formation of a twisted intramolecular charge transfer state (TICT) is found energetically feasible since the activation barrier is lower than 7 kJ mol^{-1}. The variation of the calculated transition energies from the TICT state to the corresponding Franck–Condon ground state is in very good agreement with the slope found in the Lippert–Mataga plot of *p*-DMABN. Calculated dipole moments also agree with experimental values. The numerical SCRF method turned out to give a description of excited state properties of *p*-DMABN in solution that is superior to previously applied theoretical methods based on the Onsager and the solvaton model. © 1997 Elsevier Science S.A.

Keywords: Photoinduced electron transfer; TICT; *p*-DMABN; Solvation effects; Self-consistent reaction field; SCRF

1. Introduction

Since the first observation of dual fluorescence of *p*-(dimethylamino)-benzonitrile (*p*-DMABN, Scheme 1) by Lippert and coworkers [2,3] in 1961, many experimental and theoretical studies have been performed to explain this phenomenon. Based on the spectroscopic behaviour of a series of model compounds in 1973 the so-called twisted intramolecular charge transfer state (TICT) model was proposed [4–8]: after excitation into a locally excited state, the dimethylamino group rotates from the planar conformation into a perpendicular conformation, and, in addition to this rotation, a charge transfer occurs from the dimethylamino group to the aromatic system, leading to the formation of the TICT state. Radiative deactivation of the locally excited state gives rise to fluorescence with a normal Stokes shift, whereas emission from the TICT state is responsible for the anomalous, bathochromically shifted fluorescence (see Scheme 2). While in the initial proposal, the rotation of the amino group was considered the major contribution to the reaction coordinate ξ, it was later on pointed out that other internal coordinates like rehybridisation of the amino group are of great importance as well as solvent reorganisation [9].

Besides this model, various others have been proposed since 1961. Varma and coworkers (see [10,11] and references cited therein) pointed out the importance of specific solvent–solute interactions, which can lead to red-shifted exciplex fluorescence next to the normal fluorescence. On ground of stationary and especially time-resolved fluorescence studies on a large number of model compounds, Zachariasse and coworkers [12–17] established that the TICT-model cannot provide an answer for all experimental facts. They emphasized the importance of a small energy gap between the ^1L_a and ^1L_b state as a necessary prerequisite for the appearance of dual fluorescence. In that case, the umbrella motion of the amino group leads to a strong coupling of the

* Corresponding author. Fax: +49-9131-858307.

[1] Now at Computer Chemie Centrum, Institut für Organische Chemie, Universität Erlangen-Nürnberg, Nägelsbachstr. 25, 91052 Erlangen, Germany

PII S1010-6030(96)04568-6

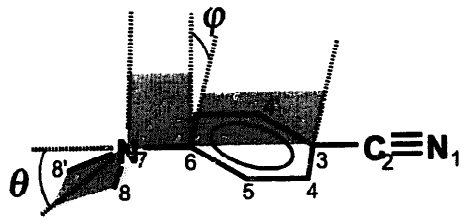

Scheme 1. Numbering of atoms (cf. ref. [1]) and definition of torsional angle φ and pyramidalisation angle θ for *p*-(dimethylamino)-benzonitrile (*p*-DMABN).

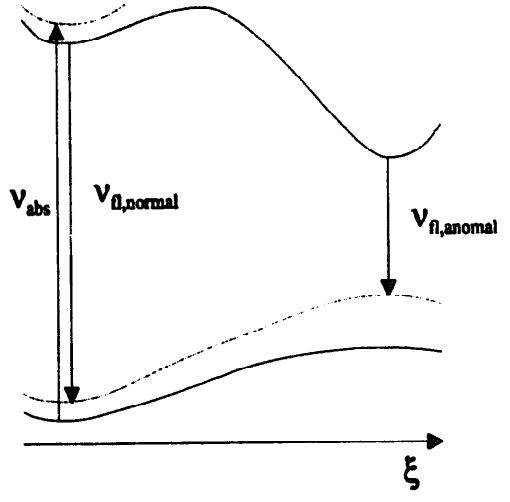

Scheme 2. Potential free energy curves describing the photophysical behavior of *p*-DMABN in solution. The solid lines represent the situation, in which the solvent cage is at equilibrium with the charge distribution of the solute in the corresponding electronic state. The dashed lines represent the 'non-equilibrium' situation (Frank–Condon state), in which the solvent cage equals the equilibrium arrangement of the other electronic state of the solute. The reaction coordinate ξ involves internal degrees of freedom (internal rotation, rehybridization) and solvent reorganization.

two lowest excited singlet states and concomitantly to a population equilibrium. Due to the more polar character of the S_2 state, the energy difference and, therefore, the strength of the coupling is a function of the solvent polarity (solvent induced pseudo Jahn–Teller coupling) [14,15]. Later on, Zachariasse and coworkers postulated that the anomalous fluorescence is caused by a more planar intramolecular charge transfer species with quinoide structure in an equilibrated solvent cage [16,17].

In addition to abundant experimental work, a great number of theoretical studies on *p*-(dimethylamino)-benzonitrile and related molecules have been carried out at different levels of sophistication. On the basis of the different approaches used, these studies can be divided into three groups. In the first class, the excited states are calculated in vacuo only [5,18–23], whereas in the second and third class solvation effects are included in different approximations, either on the basis of the continuum model [24–29,1] or in a supermolecule approach [30,31].

The earliest calculations for the isolated molecule were presented in 1976 by Khalil et al. [18] applying a CNDO/S-CI program. They were not able to prove the validity of the TICT-model. In contrast to their result, Rittig and Bonačić-Koutecký [19] claimed to find a TICT state using a modified CNDO/S-CI program and ab initio STO-3G calculations. Applying the PPP method Grabowski et al. [5] and Cowley and Peoples [20] found a low lying TICT state, and so did LaFemina et al. [21] using a CNDO/S3 program. Recently, Serrano-Andres et al. [22] carried out extensive ab initio calculations using the (CAS) SCF method in combination with multiconfigurational second order perturbation theory (CASPT2). They compared the different behaviour of *p*-DMABN and *p*-(amino)-benzonitrile (*p*-ABN), which in contrast to *p*-DMABN does not show dual fluorescence. In addition to earlier studies, they not only examined the influence of the torsional angle on the excited state properties, but also looked at the effect of the pyramidalisation of the amino group. Their results support the TICT model, while motion along the pyramidalisation coordinate cannot produce a charge transfer state that could be responsible for the anomalous fluorescence. With the same ab initio method, Sobolewski and Domcke [23] determined optimized excited state geometries, and found evidence for a possible importance of the bending of the cyano group. Such a bending would cause a stabilisation of an intramolecular CT state that is formed by transferring an electron from an aromatic π orbital to the quasi-π^* in-plane orbital of the cyano group (see Scheme 3c). The surprising result of this interesting model calculation still needs to be dealt with by theoretical methods that take into account the interaction with the solvent.

In the second class of calculations, the solute–solvent interaction was incorporated in the framework of the continuum models of Onsager [32] and McRae [33]. For the calculation of the solvaton energies, the complex solute–solvent interaction was accordingly reduced to that of a point dipole in a spherical solvent cage surrounded by a polarisable dielectric continuum. Lipiński et al. [24] calculated the excited state energies of *p*-(dimethylamino)-benzonitrile in the planar and the twisted conformation using a modified INDO method. Later on Majumdar et al. [25] used the same procedure, but optimized the ground state geometries for different rotational angles of the dimethylamino group using the MNDO method. Then the excited states were calculated with the CNDO/S-CI method. Lately, Soujanya et al. [26] used the AM1 method for the optimisation of the ground state and the calculation of the excited state properties. In all these studies the TICT model was confirmed in that a large stabilisation of the 90° twisted conformation was obtained versus the planar locally excited state. The calculated slope in the Lippert–Mataga plot is, however, much too large.

A different approach was used by Marguet et al. [27], who calculated the solvation energies after a CS INDO MRCI calculation with the solvation model. The same method was used by Gorse and Pesquer [28,29] on the basis of an AM1

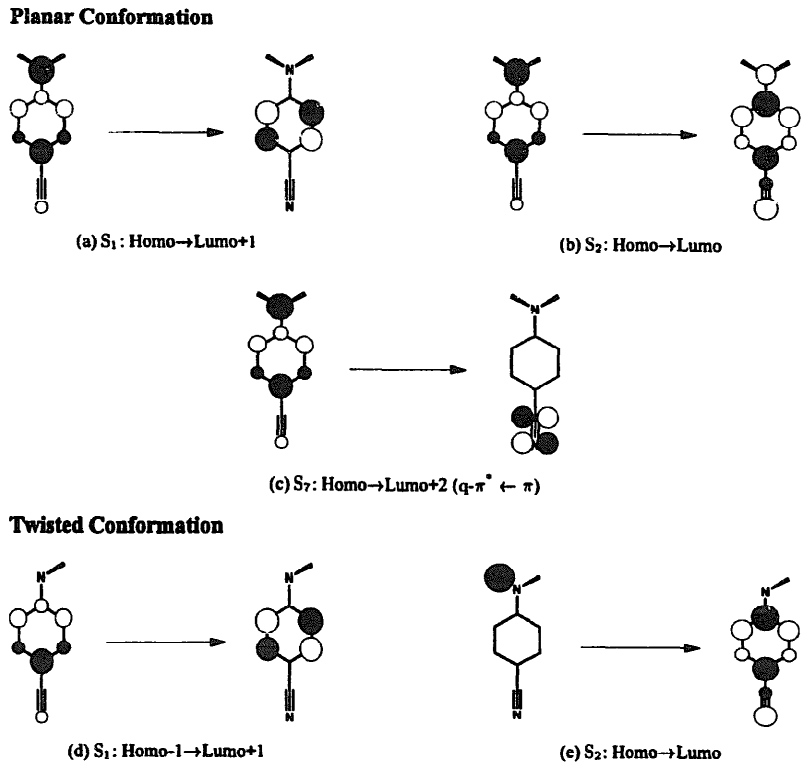

Scheme 3. Transitions of the two lowest singlet excitations of *p*-DMABN in the planar and twisted conformation. The transitions which have the largest contribution in the CI-calculation are drawn. See also Table 2.

calculation. The major drawback in these calculations is the fact that the solvation energy of the Franck–Condon state reached by CT emission turns out to be independent of solvent polarity.

Broo and Zerner [1] carried out SCRF calculations with the ZINDO program package [34] using modified Fock operators, which allow the direct calculation of excited state energies and transition energies in solution without using CI methods. Although in these calculations the slope of the anomalous fluorescence in the Lippert–Mataga plot is reproduced fairly well, the stabilisation of the TICT state is very large.

The calculations of the second class simulate the solvent by a structureless, dielectric continuum, that means specific solute–solvent interaction are not taken into account. This is possible with the supermolecule model of the third class. So far, only Kato and coworkers [30,31] carried out Monte Carlo/molecular dynamics calculations of *p*-DMABN in water. In contrast to previous work, they found a fairly small free energy of formation for the TICT state of approximately 7 kJ mol^{-1}.

Two more studies should be mentioned here. The work of Hynes and coworkers [35–37] focuses on the dynamics of TICT state formation. By applying a nonequilibrium description of solvation, they determined a two-dimensional potential energy surface, involving both the twist coordinate and a solvent coordinate. With this surface they calculated reaction paths and rate constants for the TICT state formation. The results are in good agreement with experimental observations. Polimeno et al. [38] used a totally different approach. From fitting simulated to experimental emission spectra, they obtained rather small energy differences between the TICT and the locally excited states.

With the exception of the calculations of Broo and Zerner [1], the solvent effect was taken into account after the SCF-CI calculation in all calculations cited so far. In this contribution we will present the results of self consistent reaction field (SCRF) calculations in which, following the work of Tomasi and coworkers [39–42], the interaction of the solute with the reaction field is taken into account in the SCF iteration using a modified Fock operator. Moreover, the shape of the molecule is considered by a solvent cage which is not spherical but follows the van der Waals surface of the molecule. Also, the charge distribution of the solute is described by a multipole expansion and is not reduced to a point dipole. To calculate transition energies a nonequilibrium description of the solvation energy was used. The method is described in detail in Section 2. It is applied to investigate the effect of solute–solvent interaction and of the conformation of the dimethylamino group on the properties of *p*-DMABN in the ground and excited states. The results are presented in Section 3.

Although the results of most prior calculations are qualitatively consistent with the TICT model, most of them are quantitatively not good enough to prove or disprove its validity in case of *p*-DMABN. This will be shown in detail in Section 4, in which the results of this study are discussed in comparison with prior results and experimental observations.

2. Computational method

2.1. Calculation of ground state solvation energies

In the discussion of the thermodynamic equilibrium constant or the rate expression provided by the transition state theory the relevant thermodynamic qualities are the free reaction energy ΔG^0 and the free activation energy $\Delta G^{\neq}$, respectively. From quantum mechanical model calculations, only the values for the corresponding enthalpies ΔH^0 and $\Delta H^{\neq}$ can be derived. Usually it is therefore assumed that the contribution $T \times S$ is approximately constant along the reaction coordinate, at least as long as no bonds are broken or formed. Under this assumption for the isolated molecule the change in free energy can be approximated by the corresponding changes in enthalpy. The effect of the interaction with the solvent is estimated by calculating $\Delta G_{\text{tot}}^{\text{solv}}$ in dependence on the reaction coordinate, and taken into consideration in the discussion of kinetic aspects by adding these values to those calculated for the enthalpies of the isolated molecules.

All calculations were performed with the semiempirical MO program package VAMP [43,44], using the AM1 model hamiltonian [45]. The effect of the solvent was taken into account using a numerical self-consistent reaction field (SCRF) model for ground and excited states. In this model, the free energy of solvation ($\Delta G_{\text{tot}}^{\text{solv}}$) is described as the sum of the electrostatic interaction of the solute with the induced reaction field ($\Delta G_{\text{estat}}^{\text{solv}}$), the dispersion interaction of the solute with the continuum ($\Delta G_{\text{disp}}^{\text{solv}}$), and the free cavity energy ($\Delta G_{\text{cav}}^{\text{solv}}$).

$$\Delta G_{\text{tot}}^{\text{solv}} = \Delta G_{\text{estat}}^{\text{solv}} + \Delta G_{\text{disp}}^{\text{solv}} + \Delta G_{\text{cav}}^{\text{solv}} \tag{1}$$

The solvent cage is represented by a polyhedron with a finite set of faces, also called surface elements s_i, located approximately at the van der Waals surface of the molecule. This approach has the advantage over spherical or ellipsoidal cavities that it is suitable for irregularly shaped molecules and that it can thus take into account conformational changes in the molecular structure. The molecular electrostatic potential V, which is calculated using the NAO/PC-model [46], induces a polarisation in the solvent. Within a homogeneous dielectric material there can be no induced charges. As a consequence of the different susceptibility inside and outside the cavity, an inhomogeneous charge distribution is, however, induced at the surface of the cavity. This induced surface charge density $\sigma(\boldsymbol{r}_s)$ at position $\boldsymbol{r}_s$ can be expressed as

$$\sigma(\boldsymbol{r}_s) = -\alpha \boldsymbol{E}_S(\boldsymbol{r}_s)\boldsymbol{n}_s = -\alpha\left(\frac{\partial V}{\partial n}\right)_{S-} \tag{2}$$

Here, $\boldsymbol{n}_s$ is the normal to the surface element directed toward the dielectric and $(\partial V/\partial n)_{S-}$ the gradient of the molecular electrostatic potential at the position $\boldsymbol{r}_s$ in the direction of $\boldsymbol{n}_s$. For the factor α, that describes the dielectric relaxation of the solvent in an electric field, a variety of functions can be used. For the limiting case of a static electric field, the ansatz of Born [47], Kirkwood [48], and Onsager [32] was used.

$$\alpha = \frac{\epsilon - 1}{4\pi\epsilon} \tag{3}$$

Here, ϵ is the static dielectric constant of the solvent. In order to calculate only that part of the surface charge density which is due to instantaneous electronic polarisation the same expression for α is used, except that ϵ is substituted by the square of the refractive index n.

$$\alpha = \frac{n^2 - 1}{4\pi n^2} \tag{4}$$

In accordance with the approximation of the cavity by a polyhedron, a finite set of surface charges q_i is determined by

$$q_i = \sigma(s_i)\Delta S_i \tag{5}$$

Here, $\sigma(s_i)$ is the induced charge density at the centre of the surface element i that has an area ΔS_i. In addition, self-polarisation and charge compensation was taken into account to improve the quality of the reaction field [39].

In the self-consistent reaction field (SCRF) model, the influence of the solvent on the solute is treated quantum mechanically by an additional one-electron term to the Fock operator $\mathcal{F}^0$ of the solute in vacuo.

$$\mathcal{F}(j) = \mathcal{F}^0(j) - \sum_i \frac{q_i}{r_{ij}} \tag{6}$$

with r_{ij} being the distance between electron j and surface element s_i. The corresponding Fock matrix $\mathbf{F}$ in the basis of atomic orbitals is thus given by

$$\mathbf{F}_{\mu\nu} = \mathbf{F}^0_{\mu\nu} - \sum_i q_i \left\langle \mu \left| \frac{1}{r_{ij}} \right| \upsilon \right\rangle \tag{7}$$

The point charges are formally treated as s-orbitals with zero radius and the one-electron integrals substituted by two-centre two-electron integrals. The usual formulas for the two-centre integrals are adjusted accordingly.

$$\mathbf{F}_{\mu^{(\alpha)}\upsilon^{(\beta)}} = \mathbf{F}^0_{\mu^{(\alpha)}\upsilon^{(\beta)}} - \delta_{\alpha\beta}\sum_i q_i(\mu^{(\alpha)}\upsilon^{(\beta)}|s^i s^i) \tag{8}$$

The free cavity energy $\Delta G_{\text{cav}}^{\text{solv}}$, this is the energy that is needed to create the cavity, is calculated via the following expression [44]:

$$\Delta G_{\text{cav}}^{\text{solv}} = RT\left[-\ln(1-y) + \frac{3y}{1-y}r_{\text{pro}} + \left(\frac{3y}{1-y} + \frac{9y^2}{2(1-y)^2}\right)r_{\text{pro}}^2\right]$$

$$y = \frac{\pi\rho r_{\text{solv}}^3}{6}; \qquad r_{\text{pro}} = \frac{r_{\text{cav}}}{r_{\text{solv}}} \tag{9}$$

Here, r_{cav} is the radius of a sphere that has the same surface as the cavity used for the calculation of $\Delta G_{\text{estat}}^{\text{solv}}$. The solvent is described by its density ρ and the radius r_{solv} of the solvent molecules. This contribution is independent of the electronic structure of the molecule and therefore constant for all electronic states.

The dispersion interaction of the solute with the continuum $\Delta G_{\text{disp}}^{\text{solv}}$ is approximated as [44]:

$$\Delta G_{\text{disp}}^{\text{solv}} = -\frac{1}{8}\frac{\text{IP}_M \text{IP}_S}{\text{IP}_M + \text{IP}_S}\sum_l\sum_k \alpha_{lk} g_{lk}(\infty) \quad (10)$$

IP_M and IP_S are the first ionisation potentials of the molecule and the solvent. α_{lk} is the polarisability tensor, g_{lk} the so-called reaction field tensor.

The polarisability tensor α_{lk} is determined using the variation method of Rinaldi and Rivail [49]

$$\alpha_{lk} = \frac{4}{n_{el}}\sum_{j=1}^{3} O_{lj} O_{jk} \quad (11)$$

$$O_{ij} = \sum_\mu\sum_\nu P_{\mu\nu}\left[\langle\mu|x_i x_k|\nu\rangle - \frac{1}{2}\sum_\lambda\sum_\rho P_{\lambda\rho}\langle\mu|x_i|\nu\rangle\langle\nu|x_j|\rho\rangle\right] \quad (12)$$

For the calculation of the reaction field tensor the following equations are used

$$C_i \equiv -\Delta s_i \frac{1}{4\pi}\left(1-\frac{1}{\epsilon_\infty}\right)\left[3\mathbf{r}_i(\mathbf{r}_i\mathbf{n}_i)\frac{1}{r_i^5} - n_i\frac{1}{r_i^3}\right] \quad (13)$$

$$\vec{g} = -\sum_i \frac{C(\mathbf{r}_i)\otimes\mathbf{r}_i}{|\mathbf{r}_i|^3} \quad (14)$$

C_i describes the reaction of the dielectric continuum on dipolar fluctuations at the centre of the molecule. As can be seen from these equations the electronic properties enter the calculation of $\Delta G_{\text{disp}}^{\text{solv}}$. Therefore, $\Delta G_{\text{disp}}^{\text{solv}}$ depends on the electronic state of the molecule.

2.2. Calculation of excited state solvation energies

The SCRF method was also extended for the treatment of excited states. To calculate the energetic properties of an excited state, its energy of solvation must be calculated in a reaction field that is induced by the charge distribution of this state. The first-order correlated density matrix is used to compute the electrostatic component of the total energy of solvation and to determine the polarisability tensor for the dispersion contribution. While this case corresponds to that of full relaxation of the solvent molecules, the calculation of absorption and emission spectra requires a division of the solvent cage polarisation into an orientational and an electronic component. The orientational relaxation of the solvent molecules is too slow to follow the fast absorption process. In order to calculate the properties of the Franck–Condon state, complete electronic relaxation is assumed, whereas the orientation polarisation corresponds still to that induced by the ground state charge distribution of the solute.

Rauhut et al. [44] already had implemented in the program an algorithm to calculate absorption spectra in an approximation first proposed by Bonaccorsi et al. [40]. But, as can be shown, this ansatz is only suitable for the calculation of transition energies between states that have a comparable charge distribution. Therefore, it was necessary to implement an improved approximation which is based on a nonequilibrium description of solvation. This was first done by Marcus [50]. Later, Kim and Hynes [51,52] extended this approach by taking into account the different time scales of the relaxation of the electronic and orientational polarisation.

Aguilar et al. [41] were the first to apply the latter approximation in the framework of a numerical SCRF-model. According to these authors, the change of free enthalpy of solvation of the Franck–Condon state S_E^{FC}, that is formed by the vertical transition $S_E^{FC} \leftarrow S_A$, can be calculated as

$$\Delta G^{\text{solv}}(S_E^{FC}|S_E^{FC} \leftarrow S_A) = \frac{1}{2}\sum_i [q_{e,i}^E + q_{or,i}^A] V(s_i,\rho^E) \quad (15)$$

$$-\frac{1}{2}\sum_i q_{or,i}^A [V(s_i,\rho^A) - V(s_i,\rho^E)]$$

Here, $q_{e,i}^E$ is that part of the surface charge q_i that is due to the electronic polarisation caused by the charge distribution ρ^E of the final state. The orientational polarisation described by $q_{or,i}^A$ is not able to adjust to the new charge distribution and is therefore determined from the charge distribution ρ^A of the initial state. $V(s_i,s^A)$ and $V(s_i,\rho^E)$ are the molecular electrostatic potentials in the initial and final states at the location of the surface elements s_i. If the two electronic states have equal charge distributions, the second term in Eq. (15) becomes zero and the resulting equation is the same as obtained from an equilibrium approach.

The $q_{e,i}^E$ are calculated by means of Eqs. (2)–(5), using α expressed as a function of the square of the refractive index n^2. The orientational part of the induced surface charge is calculated from the equilibrium solvated state surface charges q_i via [44]:

$$q_{or,i}^A = \left(1 - \frac{n^2-1}{n^2}\frac{\epsilon}{\epsilon-1}\right) q_i^A \quad (16)$$

2.3. Calculation of the excited state potential curves of p-DMABN

As mentioned above, the energetic and electronic properties of the ground state of *p*-DMABN were calculated with the program package Vamp 5.5 [43] using the AM1 hamiltonian [45]. The dependence of the calculated properties on the geometry of the dimethylamino group was studied by systematically varying the torsional angle φ and the dihedral angle θ (see Scheme 1). The torsional angle φ was varied in steps of 5° between 0° and 90°, the dihedral angle θ with the same stepsize between 0° and 75°. All other geometrical parameters were fully optimized. Further calculations were carried out using the thus produced geometries.

To obtain the energies and electronic properties of the excited states, for each conformation a CISD calculation was carried out using all single and double excitations from the 5 highest occupied to the 5 lowest unoccupied orbitals. It was necessary to include these 10 orbitals in order to guarantee that the same orbitals were considered in the CISD calculations for the whole conformational space (in total 876 con-

figurations were included). For optimisation of the excited state geometries, CISD calculations with 3 occupied and 3 unoccupied orbitals were performed.

The effect of solvents with different polarity, ranging from the nonpolar hexane to the polar acetonitrile, on the ground and excited state energies was studied using the numerical SCRF-method described in the previous section. The same method was used to calculate the solvatochromic shift of the absorption and emission energies.

3. Results for *p*-(dimethylamino)-benzonitrile

3.1. Electronic ground state — conformations and energies

The results of the AM1 ground state calculation of *p*-DMABN are summarized in Table 1. The minimum energy conformation has C_s symmetry. The torsional angle φ of the dimethylamino group is approximately zero; the nitrogen of the amino group has a pyramidalisation angle θ of 25°. These results are in good agreement with most other theoretical studies and most important, with the experimental findings. Only MNDO calculations [25] predict a ground state minimum for a conformation with a torsional angle of 50°. But, as was already shown by Gorse and Pesquer [28], this failure is due to shortcomings of the MNDO method in describing amino groups. All experiments, both crystallographic [53,54] and spectroscopic [21,55–58] investigations, as well as extensive theoretical ab initio calculations [22,30] agree on the fact that the dimethylamino group is not twisted but slightly pyramidalised. If one compares the calculated bond lengths and angles with the crystallographic data, the best agreement was obtained from the (CAS) SCF calculations. The AM1 calculation is found to be second best. None of the calculations predicted the shortening of the C_6–N_7 bond correctly.

The variation of the potential energy of the isolated molecule as a function of the pyramidalisation angle θ and the torsional angle φ is shown in Fig. 1a. As can be seen from the diagram, the ground state potential energy surface shows a shallow double minimum with respect to the pyramidalisation angle. The energy required for planarisation of the dimethylamino group is practically zero (≈ 1 kJ mol^{-1}). In contrast, the energy barrier for twisting is 10.5 kJ mol^{-1}, a value much lower than that reported by Soujanya et al. [26] (28 kJ mol^{-1}). This discrepancy can be understood if one considers the fact that Soujanya et al. assumed a planar dimethylamino group for the twisted conformation. This assumption is incorrect, since the pyramidalisation angle θ even increases from 25° to 45° during the rotation. The conclusion of Soujanya et al., that torsion is not free in the ground state, is still valid. As can be seen from the calculated Boltzmann distribution (Fig. 1a) only torsional angles up to $\varphi = 30°$ are thermally accessible.

In this context, a comparison with calculated properties of dimethylaniline (DMA) is interesting. In DMA, the barrier of rotation is 5.5 kJ mol^{-1}, the pyramidalisation angle increases from 31° in the planar to 45° in the twisted conformation. This result indicates that the interaction of the nitrogen with the aromatic π-system is larger for *p*-DMABN due to the electron withdrawing effect of the *para*-substituted cyano group. This is also reflected in the larger decrease of

Table 1
Comparison of crystallographic and calculated structure of *p*-DMABN [a]

	Exp. 301 K Ref. [53]	Exp. 301 K Ref. [54]	MNDO Ref. [25]	INDO/1 Ref. [1]	AM1	STO-3G Ref. [30]	(CAS)SCF Ref. [22]
Bond lengths in Å							
N_1–C_2	1.145	1.152	1.162	1.200	1.164	1.157	1.157
C_2–C_3	1.434	1.425	1.425	1.424	1.419	1.458	1.446
C_3–C_4	1.388	1.388 [b]	1.412	1.402	1.403	1.394	1.399
C_4–C_5	1.370	1.367 [b]	1.401	1.389	1.387	1.379	1.391
C_5–C_6	1.400	1.395 [b]	1.427	1.407	1.419	1.402	1.406
C_6–N_7	1.367	1.356	1.408	1.399	1.400	1.446	1.388
N_7–C_8	1.456	1.448 [b]	1.466	1.422	1.439	1.486	1.460
Bond angles							
C_3–C_4–C_5	—	121.1 [b]	120.6	121.0	120.7	120.8	120.0
C_4–C_5–C_6	—	121.5 [b]	121.7	120.2	120.9	121.1	121.4
C_5–C_6–N_7	—	121.7 [b]	121.6	120.5	121.1	121.5	121.3
C_6–N_7–C_8	121.6	121.1	121.2	120.1	118.2	122.4	122.2
C_8–N_7–$C_{8'}$	116.4	122.0	117.6	119.8	117.0	115.1	115.6
Dihedral angles							
C_5–C_6–N_7–C_8	11.9	5.4 [b]	—	0.0	16.0	23.7	21.2
Pyramidalisation angle							
θ	17.4	8.7	planar	planar	25.0	41.8	35.9

[a] For the numbering of the atoms see Scheme 1.
[b] Mean value of experimental data.

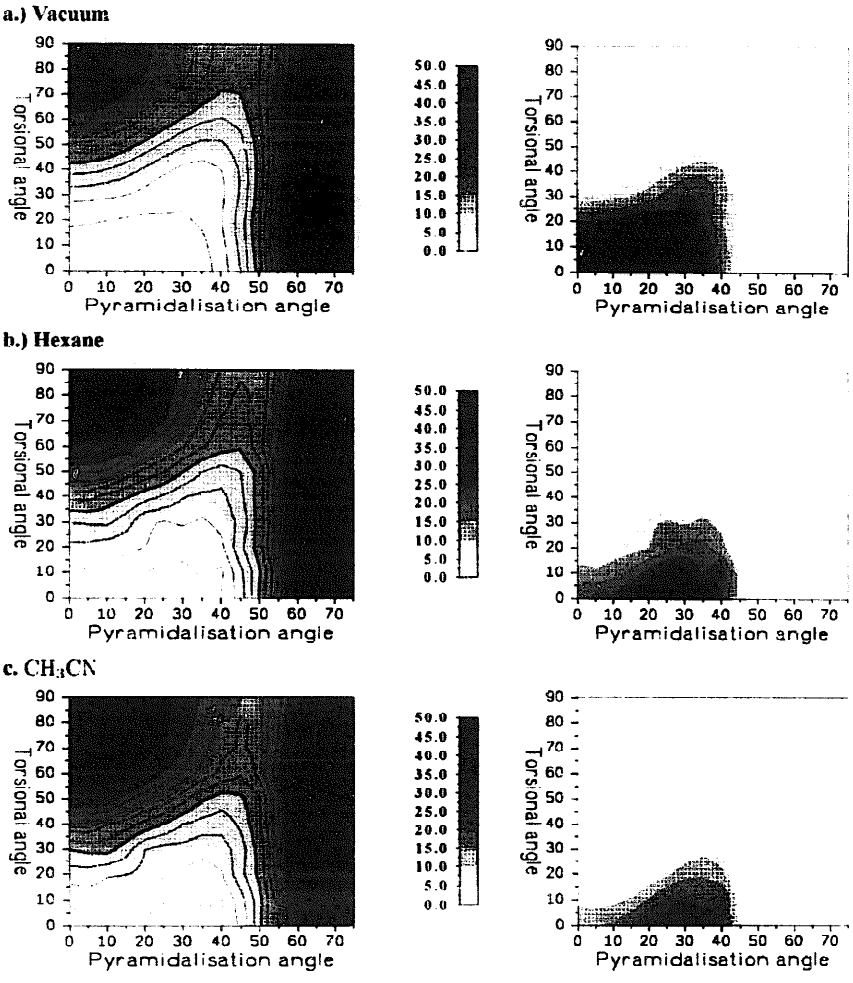

Fig. 1. Influence of the solvent polarity on the ground state free energy surface of *p*-DMABN. The energy difference relative to minimum is given in kJ mol^{-1}. Isoenergetic lines are drawn every 2 kJ mol^{-1} (thin lines) and 10 kJ mol^{-1} (thick lines). On the right side, the calculated Boltzmann distributions at room temperature are shown.

the ground state dipole moment upon twisting, namely from 17.8×10^{-30} Cm (5.4 D) to 12.0×10^{-30} Cm (3.6 D) in *p*-DMABN; in DMA the decrease is only 1.8×10^{-30} Cm (0.5 D).

3.2. Influence of solvent polarity on the ground state properties

As was mentioned in the previous section, *p*-DMABN is more polar in the planar than in the twisted conformation. Therefore, the solvation energy should be larger for the planar conformation. The results of the SCRF calculation of *p*-DMABN in hexane and in acetonitrile shown in Fig. 1b and c confirm this assumption. The energy barrier $\Delta G^{\neq}$ for rotation increases from 10.3 kJ mol^{-1} in vacuo, to 12.4 kJ mol^{-1} in hexane and 14.4 kJ mol^{-1} in acetonitrile. At the same time the distribution of torsional angles populated at room temperature narrows to $\pm10°$, that of the pyramidalisation angle to about $25\pm10°$.

The charge distribution is also influenced by the reaction field induced by the solvent. In the planar conformation, the dipole moment increases from 17.8×10^{-30} Cm (5.3 D) in vacuo to 22.4×10^{-30} Cm (6.7 D) in acetonitrile. Due to the smaller polarisability, this increase is smaller in the twisted conformation, namely from 12.0×10^{-30} Cm (3.6 D) in vacuo to 14.7×10^{-30} Cm (4.4 D) in acetonitrile. Experimental, values of 18.4×10^{-30} Cm (5.5 D) [59] and of 22.4×10^{-30} Cm (6.6 D, dioxane) [13] were reported. The calculated dipole moments are, therefore, in good agreement with the experimental results.

3.3. Properties of excited states in vacuo

In Table 2, the excited state properties for a planar ($\varphi=0°$, $\theta=25°$) and a twisted ($\varphi=90°$, $\theta=45°$) conformation are reported. These conformations correspond to the ground state minimum and the ground state transition state for rotation. The calculated energies of the lowest three excited singlet states are shown in Fig. 2 in dependence on the pyramidalisation angle θ and the torsional angle φ. The potential energy surface of the state, which is marked as LE (locally excited) in Fig. 2, is similar to the ground state potential energy surface; but in comparison to that, the minimum is more pronounced. The global minimum has a torsional and a pyr-

Table 2
Calculated properties of the lowest excited singlet states of *p*-DMABN

State S_i [a]	Energy $\Delta E(S_i \leftarrow S_0)$	Properties [b]	Character [c]	Polarization
Planar geometry ($\varphi = 0°$, $\theta = 25°$)				
S_0 ($^1A_1$)		$\mu = 17.4 \times 10^{-30}$ Cm		
S_1 ($^1B_2$)	28 740 cm^{-1}	$\mu = 21.9 \times 10^{-30}$ Cm, $f = 0.012$	LE: ^1L_b	↔
S_2 ($^1A_1$)	32 150 cm^{-1}	$\mu = 32.3 \times 10^{-30}$ Cm, $f = 0.336$	LE: ^1L_a	↕
S_3 ($^1A_1$)	35 920 cm^{-1}	$\mu = 11.0 \times 10^{-30}$ Cm, $f = 0.025$	LE	↔
S_4 ($^1A_1$)	43 050 cm^{-1}	$\mu = 30.1 \times 10^{-30}$ Cm, $f = 0.003$	LE	↕
S_5 ($^1B_2$)	43 670 cm^{-1}	$\mu = 34.4 \times 10^{-30}$ Cm, $f = 0.298$	LE	↔
S_6 ($^1A_1$)	46 380 cm^{-1}	$\mu = 33.4 \times 10^{-30}$ Cm, $f = 0.151$	LE	↕
S_7($^1A_2$)	47 870 cm^{-1}	$\mu = 56.1 \times 10^{-30}$ Cm, $f = 0.000$	ICT: q-$\pi^* \leftarrow \pi$	
Twisted geometry ($\varphi = 90°$, $\theta = 45°$)				
S_0 ($^1A_1$)		$\mu = 11.6 \times 10^{-30}$ Cm		
S_1 ($^1B_2$)	33 250 cm^{-1}	$\mu = 11.7 \times 10^{-30}$ Cm, $f = 0.001$	LE	↔
S_2 ($^1A_2$)	36 140 cm^{-1}	$\mu = 46.4 \times 10^{-30}$ Cm, $f = 0.000$	TICT-1	
S_3 ($^1A_1$)	37 400 cm^{-1}	$\mu = 13.9 \times 10^{-30}$ Cm, $f = 0.068$	LE	↕
S_4 ($^1B_1$)	42 570 cm^{-1}	$\mu = 42.4 \times 10^{-30}$ Cm, $f = 0.125$	TICT-2	
S_5 (—)	43 100 cm^{-1}	$\mu = 20.2 \times 10^{-30}$ Cm, $f = 0.031$	σ-excitation	

[a] State symmetry assuming a pseudo-C_{2v} geometry.
[b] μ = dipole moment of S_i, f = oscillator strength.
[c] LE = locally excited state. ICT = intramolecular charge transfer state. TICT = twisted intramolecular charge transfer state.
[d] ↔, ↕ direction of the transition dipole moment (orthogonal, parallel) to the phenyl–CN axis.

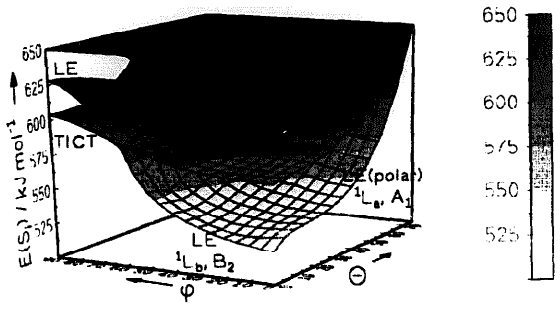

Fig. 2. Potential energy surfaces of *p*-DMABN.

amidalisation angle of 0°, the barrier for the rotation of the dimethylamino group is 75 kJ mol^{-1}. This indicates a stronger interaction of the nitrogen lone-pair with the π-system for this excited state. It can be understood if one looks at the one electron transition that has the largest contribution in the CI expansion of this state (see Scheme 3a). The electron is excited from a π orbital, which is antibonding with respect to the C–N_{amino} bond, to a π^* orbital located exclusively in the phenyl ring. Therefore, the bond order of the C–N_{amino} bond is increased, and electron density transferred from the amino nitrogen to the aromatic system. This charge shift leads to a slight increase of the dipole moment of this state of $\Delta\mu = 4.5 \times 10^{-30}$ Cm (1.4 D), whose symmetry is $^1B_2$ [2], or in Platt's [60] nomenclature, ^1L_b. The transition $^1L_b \leftarrow S_0$ with low oscillatory strength is polarized perpendicular to the long molecular axis.

The potential energy surface of the second lowest excited singlet state (marked as LE(polar) in Fig. 2) has a different shape compared to the ground and the first excited singlet state. The global minimum is again found at $\varphi = 0°$ and $\theta = 0°$, the barrier of rotation is reduced to 35 kJ mol^{-1}. The conformation with a pyramidalisation angle θ of 0° is always the lowest in energy, independently of the assumed torsional angle. A planar dimethylamino group is, therefore, preferred in this state. Compared to the ground state, the dipole moment increases considerably by $\Delta\mu = 15.0 \times 10^{-30}$ Cm (4.5 D), because significant electron density is transferred from the amino group to the cyanogroup (Scheme 3b). The strongly allowed $S_2 \leftarrow S_0$ transition is polarized parallel to the long molecular axis due to the $^1A_1$ symmetry of this ^1L_a state.

For torsional angles $\varphi > 60°$ and pyramidalisation angles $\theta < 30°$ the ^1L_a-type singlet state becomes lower in energy than the ^1L_b-type state (level crossing). For large torsional angles, the conjugative coupling between the nitrogen lone-pair and the aromatic systems vanishes. The perpendicular polarized transition $^1L_b \leftarrow S_0$ changes into a purely local excitation in the cyanobenzene fragment (Scheme 3d), while the parallel polarized transition $^1L_a \leftarrow S_0$ changes into a state which represents an intramolecular charge transfer state (Scheme 3e). The latter state can, therefore, be called a TICT state. Because of the reduced electron density at the dimethylamino cation, a planar geometry of the nitrogen is preferred (sp^2-hybridisation). Whereas in the more planar conformation the charge shift from the nitrogen to the cyanobenzene moiety can be a fraction of an elementary charge unit, it must be either 0 or 1 in the 90° conformation. From this rational it can be understood that the ^1L_b and ^1L_a, which both have charge shift character must develop into a LE state and a complete charge transfer state with a very large dipole moment. Upon transfer into a very polar solvent, the higher lying TICT state can eventually experience a so much larger

[2] To allow a comparison with the prior literature the symmetry of the electronic states was classified according to a C_{2v} symmetry of the molecule.

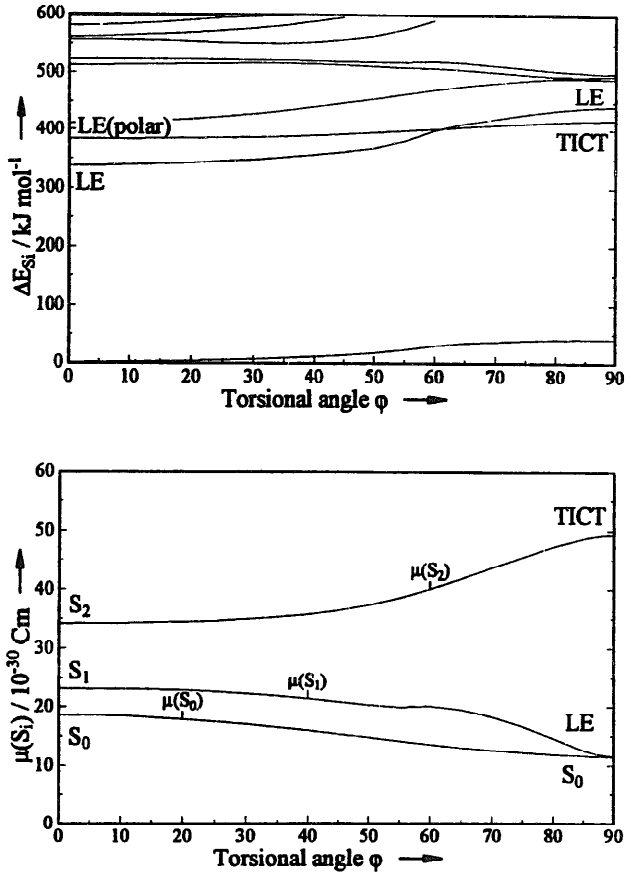

Fig. 3. Dependence of the excited state energies (top) and dipole moments (bottom) of *p*-DMABN on the torsional angle φ in vacuo. The dimethylamino group is held planar ($\theta = 0°$).

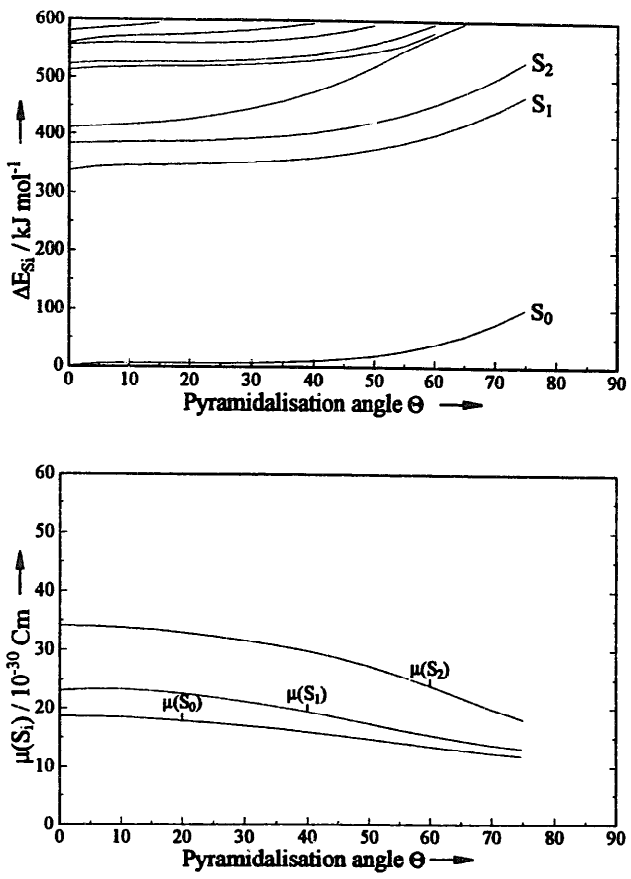

Fig. 4. Dependence of the excited state energies (top) and dipole moments (bottom) of *p*-DMABN on the pyramidalisation angle θ in vacuo. Torsional angle $\varphi = 0°$.

stabilisation that it comes to lie energetically below the LE state (Onsager model).

For the further discussion, the changes of the excited state properties along two reaction coordinates are important, namely θ and φ. In Fig. 3, the potential energy curves and the dipole moments are displayed in dependence on the torsional angle φ assuming a planar dimethylamino group. One can see that the properties of the three lowest states vary only little up to $\varphi \approx 60°$, but change rapidly for larger torsional angles. In Fig. 4, it is demonstrated that up to fairly large pyramidalisation angles no significant changes of the excited state energies and dipole moments are observed, if the torsional angle φ is chosen to be 0°. In contrast to the effect of bond rotation (Fig. 3), the dipole moment of the ^1L_a state even decreases with increasing θ. This indicates an increased decoupling of the two fragments.

Before we continue with the discussion of the results for the excited states in solution, we would like to estimate the error that arises from the fact that the excited state geometries were not optimized. To this end, the bond lengths calculated for the excited state geometries, in which all geometrical parameters except φ and θ are optimized, are summarized in Table 3. As can be seen, the bond lengths of the locally excited states (S_1 and S_2 in the planar and S_2 in the twisted conformation) change not much relative to the ground state; the average change $\Delta\bar{d} = 1/N\Sigma_{i=1}^{N}|\Delta d_i|$ is about 0.01 Å. In contrast, the TICT state shows a significant change of the bond lengths. This is reasonable if one considers the electronic character of this state. The dimethylamino group is positively charged which causes a shortening of the nitrogen carbon bond (C_6–N_7). The benzonitrile fragment carries a negative charge which is distributed across the whole ring system. This causes a lengthening of all bonds. The average change for this state is $\Delta\bar{d} \approx 0.04$ Å. An estimation of the error can now be given by using the Marcus approximation for the internal reorganisation energy λ_i, namely:

$$\lambda_i = \frac{1}{2}\sum_j \frac{2k_j^R k_j^P}{k_j^R + k_j^P}(Q_j^R - Q_j^P)^2 \tag{17}$$

If we consider only changes in bond length and assume that the force constants $k_j^{R/P}$ are independent of the state and can be approximated by an average force constant $\bar{k}$ and substitute the individual bond length changes by an average change for all N bonds, then Eq. (17) simplifies to

$$\lambda_i \approx \frac{1}{2}\sum_j \frac{2k_j^2}{2k_j}(\Delta d_j)^2 \tag{18}$$

$$\approx \frac{1}{2} N \frac{\bar{k}}{2}\Delta\bar{d}^2 \tag{19}$$

Table 3
Comparison of the optimized geometries of the three lowest singlet states of *p*-DMABN for the planar ($\varphi=0°$, $\theta=0°$) and the twisted ($\varphi=90°$, $\theta=0°$) conformations, in addition to the bond lengths, the average change of bond length of the individual states $\Delta\bar{d}$ is given [a]

	Planar conformation			Twisted conformation		
	S_0	S_1	S_2	S_0	S_{TICT}	S_2
Bond lengths in Å						
N_1–C_2	1.164	1.161	1.167	1.164	**1.175**	1.164
C_2–C_3	1.418	1.422	1.412	1.421	**1.470**	1.412
C_3–C_4	1.402	1.415	1.418	1.401	**1.453**	1.422
C_4–C_5	1.386	1.405	1.381	1.391	**1.422**	1.407
C_5–C_6	1.422	1.415	1.446	1.413	**1.443**	1.420
C_6–N_7	1.388	1.365	1.385	1.409	**1.331**	1.407
$\Delta\bar{d}$	—	0.012	0.011	—	**0.040**	0.011

[a] For the numbering of the atoms see Scheme 1.

If we evaluate Eq. (19) with an average force constant of $\bar{k}=500$ Nm^{-1} and an average change of bond length of $\bar{d}=0.03$ Å (the average difference between CT and LE states) then we obtain for eleven bonds (C–H bonds are not considered here) an internal reorganisation energy λ_i of approximately 15 kJ mol^{-1}. This is of course only a crude estimation, but it indicates that the calculated TICT state energies should be somewhat too high. The energy barrier for the torsion in the excited state should not be influenced too much, because, as can be seen from Fig. 3, the transition state for rotation is found at a torsional angle of approximately 60° and the charge transfer character only becomes dominant for torsional angles larger than 60°. Up to $\varphi\approx 60°$ an approximately constant error should be made by the calculations due to the incomplete treatment of reorganisation energy.

3.4. *Influence of solvent polarity on the excited state properties*

In Fig. 5, the effect of the solute–solvent interaction on the excited state free energies is shown. The dielectric properties of the solvents hexane, diethylether, methylenechlorid, and acetonitrile were used in the calculations. As described above for the electronic ground state, the torsional and the pyramidalisation angle were varied systematically (10° steps) and for each ground state optimized conformation the solvation free energies of the lowest excited singlet state calculated by means of Eq. (1). In addition, the conformational distribution was determined for this state assuming a Boltzmann distribution law. It should be mentioned explicitly that the excited state free energies correspond to the completely solvent relaxed state, but with a solute geometry equal to that of the equilibrium ground state solute conformation.

The free energy of the more polar ^1L_a state is lowered more by solvation than the free energy of the ^1L_b. But, this stabilisation is not sufficient in hexane ($\epsilon=1.8863$) to bring down the ^1L_a below the ^1L_b. The crossing of the two surfaces is, however, shifted from $\varphi\approx 60°$ in vacuo to 40° because of the opposite change of the dipole moment of these two states with increasing angle φ (cf. Fig. 3). The planar or only slightly twisted conformation is energetically preferred. The free energy of rotation including the change of electronic state is reduced from 75 kJ mol^{-1} in vacuo to 21 kJ mol^{-1}.

In diethylether ($\epsilon=4.335$), the ^1L_a state is already the lowest excited state independently of the conformation of the dimethylamino group. As has been shown in the previous section, the dipole moment of this state is much larger for conformations around $\varphi=90°$. Therefore, the solvation of this state must be considerably larger for torsional angles around 90° than for the planar conformation. The energy difference between the planar ($\varphi=0°$) and the twisted conformation ($\varphi=90°$) is essentially zero. Thus, a considerable amount of excited *p*-DMABN should be found in the twisted conformation, provided that rotation is fast enough in comparison to other relaxation processes.

This described trend continues in the more polar solvents methylenechloride and acetonitrile. According to the results of the calculation, the majority of the excited *p*-DMABN molecules should relax to a twisted conformation in methylenechloride ($\epsilon=8.93$). In the very polar acetonitrile ($\epsilon=35.94$), practically all excited molecules should end up in the twisted conformation.

The potential energy surfaces displayed in Fig. 5 suggest that for all solvents a planar dimethylamino group is energetically preferred independently of the adopted torsional angle φ. For a more quantitative analysis we can, therefore, restrict ourself to calculations with a fixed pyramidalisation angle of $\theta=0°$. This restriction was applied in many earlier theoretical studies, but has not yet been proven to be valid. The results of our SCRF calculations describing the effect of a variation of the torsional angle in steps of 5° are given in Fig. 6. The reaction free energies ΔG for a torsion from $\varphi=0°$ to 90° in the lowest excited state and the related activation free energies $\Delta G^{\neq}$ are summarized in Table 4.

In hexane, the potential energy curve of the ^1L_b state lies for small torsional angles below the potential energy curve of the ^1L_a state. Besides the global minimum at $\varphi=20°$ no other minimum is found. Especially, the ^1L_a state has a maximum at $\varphi=90°$. The energy needed for torsion (including the change in electronic state) is 21 kJ mol^{-1}. Changing to

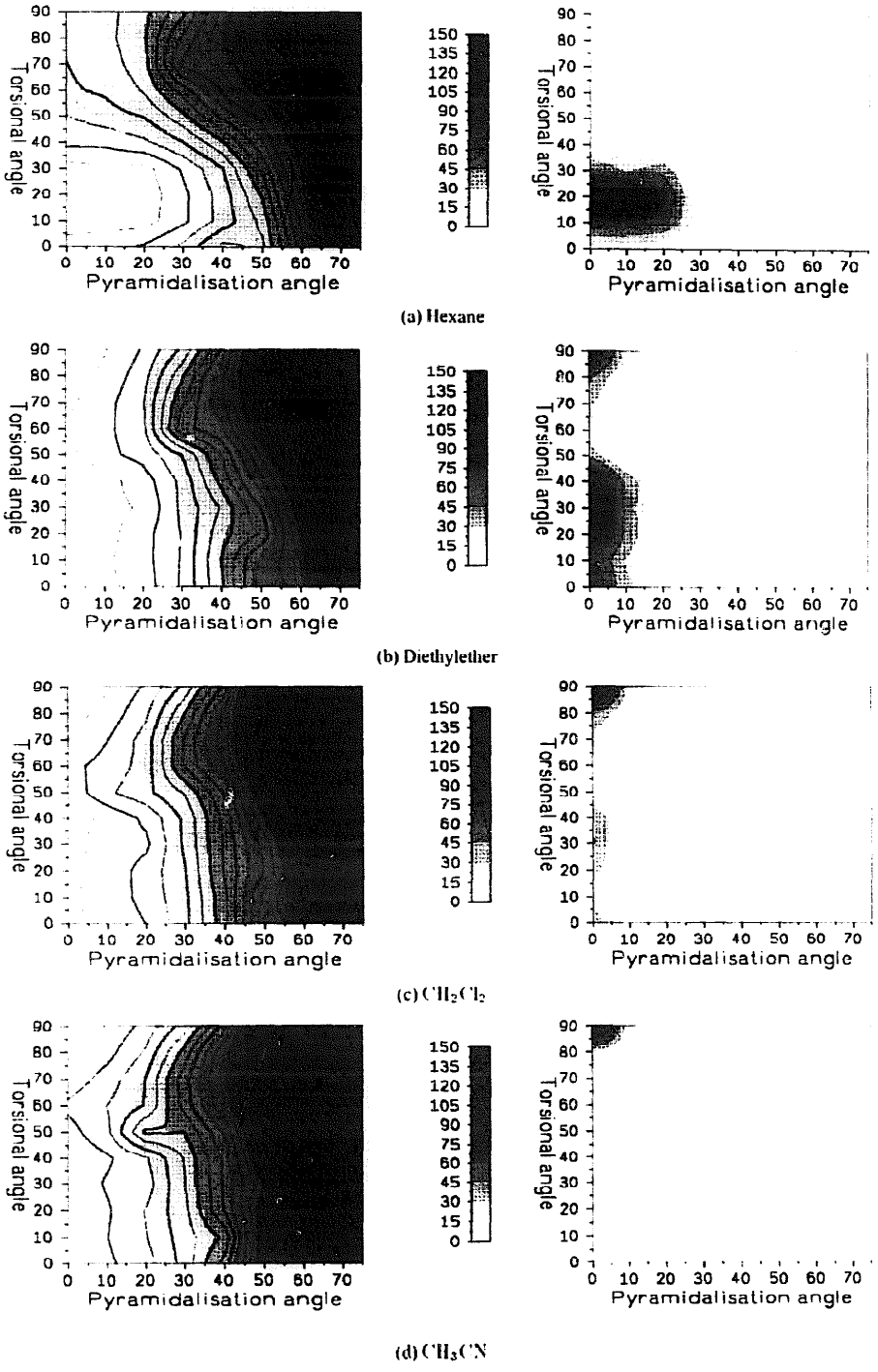

Fig. 5. Influence of solvent polarity on the energetics of the lowest excited singlet state of *p*-DMABN. The energy difference to the global minimum of the state is given in kJ mol^{-1}. Isoenergetic lines are drawn every 2 kJ mol^{-1} (thin lines) and 10 kJ mol^{-1} (thick lines). On the right side, the calculated Boltzmann distributions at room temperature are shown.

solvents of medium polarity, the ^1L_a state is already lowered below the ^1L_b state for all torsional angles. Further, a second, local minimum appears at $\varphi = 90°$, which is only 1 kJ mol^{-1} above the global minimum at $\varphi \approx 35°$. Since in the ground state, torsional angles around 0° are preferred, a more or less planar conformation should be populated shortly after excitation. The calculated activation free energy for the torsion is small enough (6 kJ mol^{-1}) to allow the establishment of a rapid equilibrium between conformations with a nearly planar and a twisted conformation. In polar solvents, the twisted conformation represents the global minimum in the potential energy curve. In methylenechlorid, the free energy difference is negligible (0.5 kJ mol^{-1}). Again, the activation barrier is small enough (6.5 kJ mol^{-1}) to allow the formation of a fast equilibrium between both conformations. In the very polar acetonitrile, the twisted conformation lies already 6 kJ mol^{-1} below the planar one, the thermodynamic equilibrium is therefore almost totally shifted to the twisted conformation.

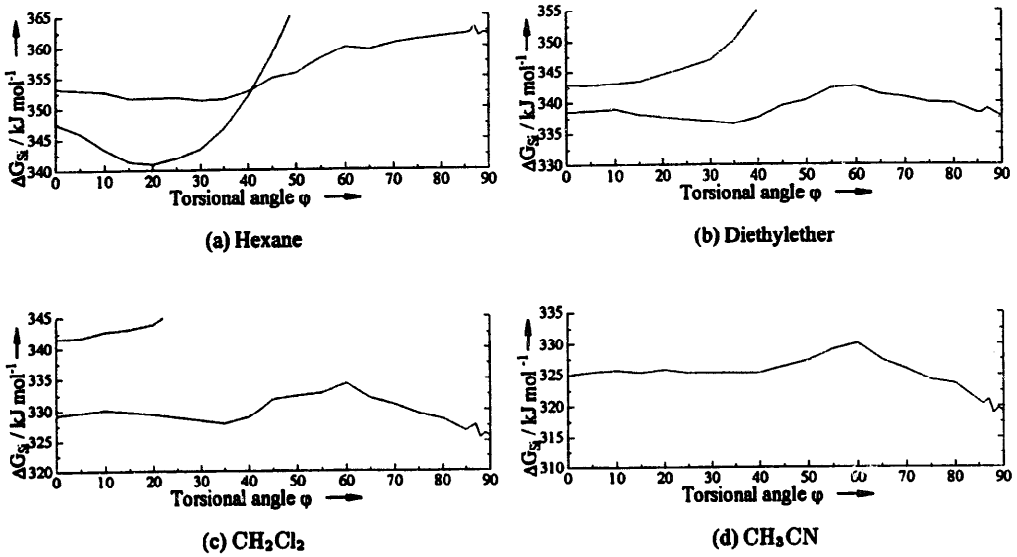

Fig. 6. Effect of torsion on the singlet excited state free energies in different solvents. The dimethylamino group is held planar ($\theta = 0°$).

Table 4
Dependence of $\Delta G^{\neq}$ [a], ΔG [b], and ground and excited state dipole moments of *p*-DMABN on the solvent polarity.

Solvents	$\Delta G^{\neq}$ (kJ mol^{-1})	ΔG (kJ mol^{-1})	μ_{S_0} ($\times 10^{-30}$ Cm)	$\mu_{S_{LE}(\omega)}$ ($\times 10^{-30}$ Cm)	$\mu_{S_{TICT}}$ ($\times 10^{-30}$ Cm)
Vacuum	—	75	19.1	—	49.4
Hexane	—	21	22.6	—	51.1
Diethylether	5.9	1.1	22.8	39.5	52.1
CH_2Cl_2	6.4	−0.5	23.6	40.8	52.6
CH_3CN	5.1	−6.1	24.2	41.6	53.0

[a] $\Delta G^{\neq}$ is the activation free energy for the torsion from the planar to the twisted geometry in the lowest excited singlet state.
[b] ΔG is the reaction free energy for TICT state formation.

This is even more true, if the reorganisation energy is taken into account. Thus we can assume that in this solvent emission only occurs from the twisted conformation.

It is interesting to compare the calculated reaction free energies with experimental results. From ps time-resolved fluorescence measurements Hicks et al. [61] deduced reaction free energies between the two emitting states ranging from 4 kJ mol^{-1} in medium polar to −7 kJ mol^{-1} in very polar solvents. Similar results were obtained by Heisel and Miehé [62] (−4 to −7 kJ mol^{-1} in nitriles) and by Leinhos et al. [12] (−10 kJ mol^{-1} in toluene). A different approach was used by Polimeno et al. [38] who simulated the emission spectra of *p*-DMABN in a variety of solvents. According to their results, the reaction free energies decrease from 27 kJ mol^{-1} in nonpolar hexane to 2.0 kJ mol^{-1} in diethylether and −17 kJ mol^{-1} in acetonitrile. Altogether one can state that our results compare favourably with these experimental findings, whereas most other theoretical studies report much too large reaction free energies (between −50 and −100 kJ mol^{-1}). The only exception is the ab initio CI–MC study of Kato and coworkers [30,31] who obtained a reaction free energy of $\Delta G = -7.2$ kJ mol^{-1} for *p*-DMABN in water.

The experimental results regarding the height of the activation barrier between normal and anomalous fluorescing states are more controversial. Hicks et al. [61] report a considerable barrier which varies between 45 kJ mol^{-1} in medium polar solvents to 17 kJ mol^{-1} in very polar solvents. In contrast, other groups (Heisel and Miehé [62], Braun and Rettig [63]) deny the existence of a solvent polarity dependent barrier. Leinhos et al. [12] report a barrier of 7 kJ mol^{-1} in toluene. The activation barrier calculated by Kato and coworkers [30,31] is approximately 7.5 kJ mol^{-1} (in water). A comparison of the experimental results with the theoretical calculations presented here is only in so far possible, as the calculation neglects dynamic solvation effects. Therefore, the calculated activation barrier can only be an approximation of the experimental activation energy [35–37].

3.5. Calculated absorption and emission energies

Using the method outlined in Section 2.2, emission energies were calculated for the different conformations along the torsional coordinate. The results are given in Fig. 7 in which the experimentally observed emission energies are indicated (hatched areas) for easier comparison.

Two distinct ranges can be seen in which the experimental and the calculated emission energies coincide. In the first range with torsional angles between $\varphi = 0°$ and 45° are the calculated transition energies equivalent to the energy of the normal emission. The second range, which can be assigned

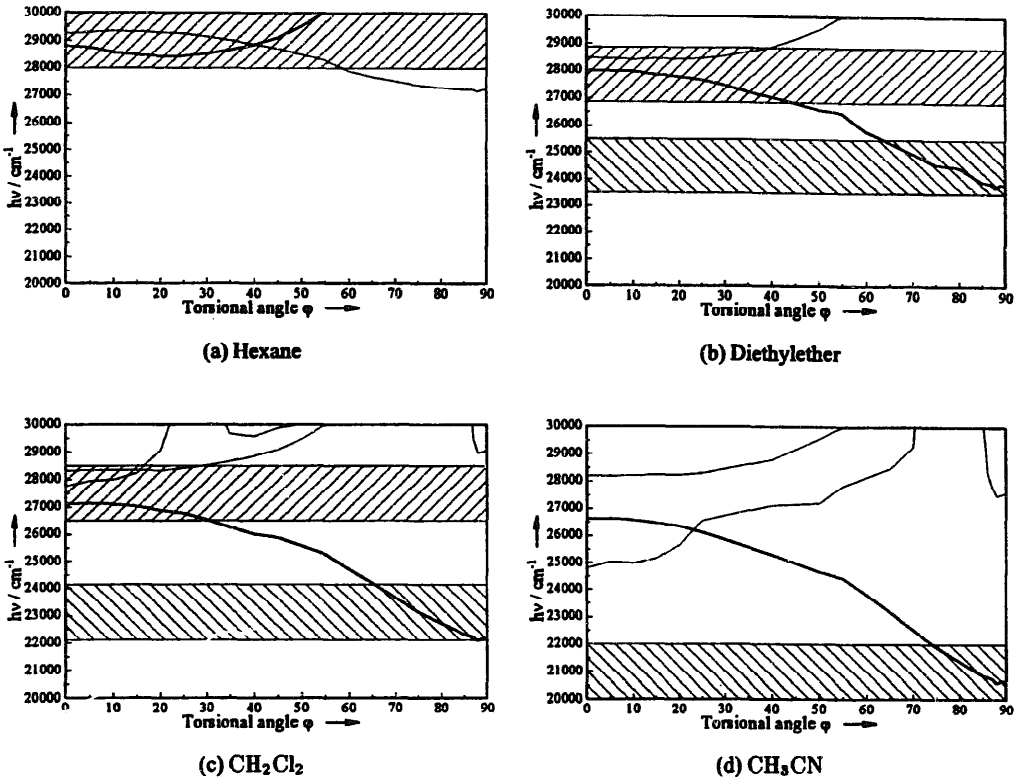

Fig. 7. Calculated emission energies of *p*-DMABN as a function of solvent polarity and torsional angle φ. The emission energy of the lowest excited S_1 state is drawn with a thick line. The range of the experimentally observed emission energies (maximum $\pm 1000\ cm^{-1}$ is hatched:

normal,

anomal fluorescence.

In all calculations, the dimethylamino group was kept planar ($\theta = 0°$).

to the anomalous fluorescence, spans torsional angles φ between 70° and 90°. This observation, combined with the results of the previous section, clearly demonstrates, that the predictions of the TICT-model are confirmed from the calculations for *p*-DMABN.

So far, the results of the SCRF-CI calculations show that normal emission occurs from excited molecules which have a more or less planar conformation ($\varphi < 45°$). The anomalous fluorescence can be assigned to molecules with a twist angle of more than 70°. Based on this consideration, we can carry out a more elaborate comparison with experimental data from a larger variety of solvents. In Table 5, the experimentally observed absorption and emission energies are compared with the calculated transition energies for two distinct conformations: (i) a planar conformation ($\varphi = 0°$, $\theta = 0°$) was used to calculate the absorption and emission energies of the normal fluorescence, (ii) a twisted conformation ($\varphi = 90°$, $\theta = 0°$) was assumed to estimate the energy of the anomalous fluorescence.

To allow for a better comparison, the results are shown in addition in Fig. 8 in the form of a Lippert–Mataga plot [3]. The calculated absorption energies are approximately $6000\ cm^{-1}$ below the experimentally determined values. The origin of this difference could be found either in an incomplete selection of configurations in the CI calculation or in a general failure of the applied hamiltonian. Evidence against the latter reason is the fact that the calculated energy difference of S_1 and S_2 state of the isolated molecule is in good agreement with the result of the ab initio (CAS) SCF calculation by Sobolewski and Domcke [23] (ab initio: $3050\ cm^{-1}$, AM1: $3400\ cm^{-1}$). Also in good agreement is the calculated charge distribution in these two states which is of course important for a proper estimate of the solvation effect.

The absorption energies to the ^1L_b state show almost no dependence on the solvent polarity, whereas the transition to the ^1L_a state experiences a bathochromic shift of $1000\ cm^{-1}$ upon changing from hexane to acetonitrile. The scattering of the experimental data as well as the small energetic difference between the two lowest, locally excited singlet states do not allow a more detailed discussion.

The agreement of the experimental and theoretical emission energies (Fig. 8) appears to be almost perfect. This fact should not be overestimated, since the contribution of the internal relaxation to the Stokes shift is not included in the

[3] In the Lippert–Mataga plots the *f*-values were calculated from the following equation [64]: $f(\epsilon,n^2) = (\epsilon-1)/(2\epsilon+1) - (1/2)n^2/(1/2)n^2+1$.

Table 5
Comparison of experimental [3] and calculated absorption and emission energies of *p*-DMABN [a]

Solvent	Experiment			Theory		
	Absorption (cm^{-1})	Emission		Absorption	Emission	
		Normal (cm^{-1})	Anormal (cm^{-1})	$\varphi=0°$ (cm^{-1})	$\varphi=0°$ (cm^{-1})	$\varphi=90°$ (cm^{-1})
Hexane	35 550	29 050	—	28 840	28 810	27 220
Benzene	34 420	28 350	sh	28 730	28 730	26 830
CCl_4	34 400	28 150	—	28 780	28 760	26 820
Diethylether	35 150	27 850	24 450	28 580	27 990	23 820
$CHCl_3$	—	—	—	28 260	27 730	23 580
Ethylacetate	34 700	27 550	22 900	—	—	—
CH_2Cl_2	35 800	27 500	23 200	27 910	27 130	22 140
Pyridine	33 900	27 400	22 200	27 620	26 870	21 850
Nitrobenzene	—	—	—	27 320	26 510	21 180
Acetone	nm	27 600	—	27 800	26 760	21 030
DMSO	—	—	—	27 449	26 520	20 930
Ethanol	34 000	—	21 100	27 650	26 540	20 880
Methanol	34 450	—	21 050	27 680	26 480	20 610
CH_3CN	—	—	—	27 220	26 610	20 620
H_2O	—	—	—	27 570	26 330	20 310

[a] For a graphical representation see the Lippert–Mataga plot of Fig. 8.
sh: shoulder; nm: not measurable.

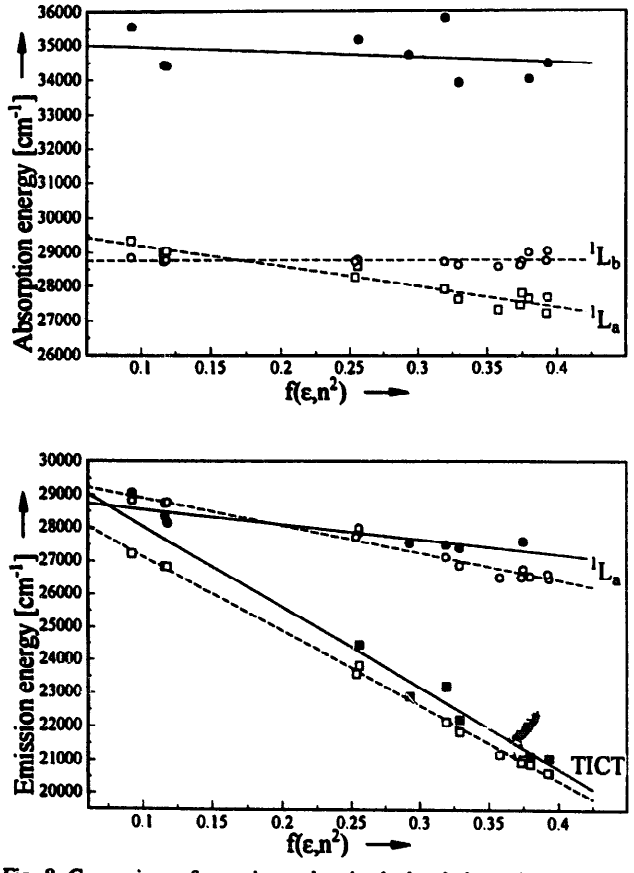

Fig. 8. Comparison of experimental and calculated absorption (top) and emission (bottom) energies of *p*-DMABN in a Lippert–Mataga plot. Symbols used: Absorption: Experimental data: ● absorption maximum. Calculated data: absorption □ $^1L_a \leftarrow S_0$, ○ $^1L_b \leftarrow S_0$. Emission: Experimental data: ● normal, ■ anomal fluorescence. Calculated data: ○ normal ($\varphi=0°$), □ anormal ($\varphi=90°$) fluorescence.

calculations. (To correctly take this into account would require the optimisation of the individual excited states which is not easily possible in the present form of the program.) The coincidence between absolute values of calculated and experimentally observed emission energies is thus due to a compensation of errors in absorption energy as discussed above and the Stokes shift due to the geometrical relaxation of internal coordinates other than those of the dimethylamino group considered in this work. Further changes in absolute transition energy could result from a possible variation of the scaling factor relating the chosen cavity size to the van der Waals surface. In accordance with previous studies on other systems [44], we have chosen a value of 1.1. What is more important than absolute values, is, however, that the experimentally observed difference between normal and anomalous fluorescence and the solvatochromic shift of both transitions is very well reproduced. This implies that the course of the potential energy curves along the selected internal coordinates is well described.

4. Discussion

4.1. Comparison with other calculations

As was already mentioned, several methods had been used in the past to calculate the photophysical properties of *p*-DMABN. In order to form an opinion of the different calculations, it is useful to look at characteristic properties of the photophysical processes involved. In particular, the extent of the solvatochromic shift of the normal and anomalous fluo-

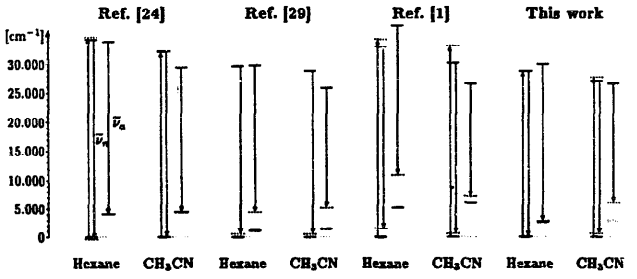

Fig. 9. Comparison of excited state free energies of different studies. In each individual diagram, the energetics of the planar conformation are given on the left, those of the twisted on the right. The energies of the solvent-equilibrated states are indicated by a solid line. The Franck–Condon nonequilibrium state is shown by a dotted line ν_n: normal emission, ν_a: anomal emission. Information taken from Lipiński et al. [24], Gorse and Pesquer [29], and Broo and Zerner [29].

rescence is of interest, since the latter can be easily compared with experimental data. Furthermore, the solvent polarity dependent amount of energy relaxation after an absorption or emission event should be considered here. With increasing polarity of the solvent, the energy difference between the initially formed Franck–Condon and the equilibrated state should increase. In addition, this energy difference should be larger for the emission than for the absorption process and larger for the anomalous than for the normal fluorescence. To allow for an easier comparison, these characteristic quantities, calculated with the different methods, are displayed in Fig. 9.

The first calculation that took solvent effects into account was carried out by Lipiński et al. [24] using the INDO/S-CI. As can be seen from Fig. 9, their method gave almost no difference between the Franck–Condon and the corresponding solvent relaxed state. This neglect of nonequilibrium solvation has an important consequence. To reproduce the experimental solvatochromic shift, the calculated stabilisation of the TICT state must become larger. Therefore, the calculated reaction energy for twisting in the excited state must turn out to be too large (≈ 35 kJ mol^{-1}).

The same line of argument is true for the CNDO/S-CI calculations of Majumdar et al. [25]. They calculated a solvatochromic shift of the anomalous fluorescence that is more than twice as large as the experimentally observed shift. Again, the calculated stabilisation of the TICT state in polar solvents must be too large (≈ 80 kJ mol^{-1}).

Soujanya et al. [26] applied, like we did, the AM1 method for the calculation of the excited states. To determine the absorption energies and the solvation energies of the different states they used the same approximations as Majumdar et al. [25]. The fluorescence energy was, however, calculated as the difference between the energies of the equilibrium solvated states. This procedure is not correct, since in order to be consistent, a similar equation as for the absorption process should have been used (Eq. (2) in [26]). As a consequence, their calculation does not treat the solvent relaxation correctly. The calculated solvatochromic shift is twice as large as experimentally observed. The energy of TICT state formation is ≈ 100 kJ mol^{-1}.

The solvaton model was first employed by Marguet et al. [27]. Recently, Gorse and Pesquer [28,29] extended the method to allow for the calculation of electronic transitions in solution. To understand their results, it is worth to describe the model more closely. A so-called solvaton is associated with each atom. In the calculation of the equilibrium solvation energy the charge of the solvaton is chosen as the opposite of the charge of the associated atom. The interaction between the solvaton and the atoms is controlled by an effective radius, which can be used as a scaling parameter to adjust the calculated results to the experimental data, as was done by Gorse and Pesquer. The calculated relaxation energies turn out to be almost independent of the solvent polarity (see Fig. 9). In particular, in nonpolar solvents, where they should be very small, they are too large. This can be understood by looking at the method that the authors employed to calculate the solvation energy of the Franck–Condon state S_i^{FC} formed after the transition $S_i^{FC} \leftarrow S_a$. Gorse and Pesquer assumed that the solvaton charges used for the calculation of S_i^{FC} are solely determined by the charge distribution of the state S_a. The relaxation of the electronic polarisation is not treated at all. As a consequence the calculated emission energies are too small. This also implies that the calculated solvent stabilisation is overestimated.

Finally, we have to consider the results of Broo and Zerner [1]. They included the influence of the reaction field in a spherical solvent cage in the Fock-operator. With different modifications of the operator they were able to calculate the energies of Franck–Condon and relaxed states directly. Although they differentiate between electronic and orientational polarisation, the differences in relaxation energies determined from their calculated excited state and transition energies show a strange solvent dependence. In nonpolar solvents, the relaxation energy turns out larger than in polar solvents (see Fig. 9). Further, the energy calculated for the normal emission is on the average 2000 cm^{-1} larger than experimentally observed, while the anomalous fluorescence is always too low in energy by 200–5400 cm^{-1}. Taken together, this indicates, that the relative energies of the excited states cannot be correct. Especially the solvent stabilisation of the TICT state should be overestimated by Broo and Zerner.

4.2. Discussion of the various models

As was already mentioned, various models have been proposed to account for the photophysical behaviour of *p*-DMABN. The first explanation by Lippert et al. [2,3] was based on the difference in dipole moment of the ^1L_b and ^1L_a state, respectively. In more polar solvents, the ^1L_a state is more strongly stabilized than the less polar ^1L_b state and consequently shifted below the latter one. This predicted behaviour is in accordance with our numerical results. The calculated transition energies between the down-shifted ^1L_a and the corresponding Franck–Condon ground state do, however, not experience the experimentally observed batho-

chromic shift (Fig. 7). Therefore, a significant alteration of the geometry must occur upon transition to the anomalous emitting state.

One intramolecular relaxation pathway that was proposed by Schuddeboom et al. [13] is the increase of the pyramidalisation angle of the dimethylamino group and connected with this a possible charge separation in the excited state. Our calculation clearly show, in accordance with other theoretical studies [29], that this does not occur (see Fig. 4). Also, no significant change of the charge distribution on planarisation of the amino group was observed.

However, the result presented above, demonstrate that torsion of the amino group accompanied with a rehybridisation (planarisation) of the amino group is a possible variation in geometry which produces a charge transfer (TICT) state, whose characteristics are in accordance with experimental findings. It must, however, be stressed that, in contrast to previous theoretical studies, the energy of formation of the TICT state is rather small (-6 kJ mol^{-1} in CH_3CN). Therefore, both the activation barrier and the energy of formation of the TICT state are sensitively dependent on structural parameters. This is reflected by SCRF calculations within the same set of approximations applied to *p*-(amino)-benzonitrile (*p*-ABN) and *p*-(methylamino)-benzonitrile (*p*-MABN). They predict that TICT formation should not occur in *p*-ABN for energetic reasons ($\Delta H \approx 25$ kJ mol^{-1}, $E_A = 35$ kJ mol^{-1}) and should be kinetically hindered in *p*-MABN ($\Delta H \approx -12$ kJ mol^{-1}, $E_A = 10$ kJ mol^{-1}) [65,66]. Similar statements can be made for *m*-(dimethylamino)-benzonitrile (*m*-DMABN) and 3,5-dicyano-dimethylaniline (DCDMA) [65,66]. Without putting too much emphasis on the absolute numbers, the presented examples should demonstrate the point that a comparison of the fluorescence behaviour of *p*-DMABN and that of any of the other model compounds cannot provide absolute evidence for or against the validity of the TICT model in the case of *p*-DMABN. Slight structural changes can alter the energetics of the excited state significantly. This is also true, in our opinion, for the observation by von der Haar et al. [16,17] that larger alkyl groups on the amino nitrogen can even increase the yield of the CT state. Photoinduced isomerisation of several compounds on a (sub-)picosecond time scale [61,67,68] gives clear evidence for fast intramolecular rotation provided the driving force is large enough. In accordance with our experience [65], Sobolewski and Domcke [23] pointed out that the energies of the locally excited states (C_{2v}-symmetry) are sensitive to alkyl substitution and so are the dipole moments. This means that the course of the potential curve will be different for the isolated molecules and even more so in solution, since the solvent cage has a different size.

Sobolewski and Domcke [23] studied the stabilisation of that CT state, which is formed by transfer of an electron from the aniline π-electronic system to the in-plane quasi π^* orbital of the cyano group (see Scheme 3c), accompanied by a bending of the cyano group. They proposed that due to the large dipole moment this state could become important in polar solvents. Whereas the vertical excitation energy to this state is about 7.2 eV for the ground state optimized geometry, the nonvertical energy difference reduces to about 4.5 eV (*p*-DMABN) and 4.63 eV (*p*-ABN) when the cyano group is bent ($\approx 120°$). In the isolated molecule this state, with a dipole moment of 54.8×10^{-30} Cm (*p*-DMABN) and 44.4×10^{-30} Cm (*p*-ABN) is consequently only 0.37 eV (*p*-DMABN) and 0.46 eV (*p*-ABN) above the $^1B_2$ state. In the ground electronic state, the destabilisation due to rehybridisation is about 1.17 eV. Both data combined yield a transition energy for CT fluorescence of 3.33 eV (*p*-DMABN) and 3.46 eV (*p*-ABN). We have performed SCRF calculations by systematically varying the torsional and the cyano bending angle of *p*-DMABN in order to study the solvent dependence of the planar intramolecular charge transfer state [66]. According to these preliminary calculations, the solvent stabilisation of this CT state is not even in acetonitrile large enough to lower its energy beneath the lowest locally excited state in the planar ground state geometry. A definite conclusion about the possible role of such a planar, but bent CT state can be made only after the effect of intramolecular relaxation of the other internal coordinates is included in the calculation.

5. Conclusion

The results presented in this contribution demonstrate that the SCRF model is suited to calculate the effect of solvation on ground and excited state energies and dipole moments. This is especially true if the variation of these quantities with changes in molecular geometry are to be estimated since the solvent cavity is shaped according to the van der Waals surface.

The modelling of the electrostatic solvent–solute interaction via the coulombic interaction between a surface charge density and the solute-s charge distribution allows an easy distinction between the effects of electronic and orientational polarisation and thus provides a convenient basis to study the interplay between intramolecular and solvent relaxation. The most important improvement with respect to fluorescence solvatochromism is the modelling of the solvent-equilibrated, geometrically relaxed excited state and that of the Franck–Condon ground state.

The results obtained for *p*-DMABN are in favour of the TICT state being the source of anomalous fluorescence. But, in contrast to previous theoretical studies, the calculated energy of formation of the TICT state is rather small. TICT state formation can therefore easily be influenced by structural changes. From this, it becomes evident that TICT formation must not be considered an a priori decay channel which is necessarily important whenever an aminogroup linked to an acceptor is capable of undergoing internal rotation.

Acknowledgements

The authors wish to thank Dr. T. Clark for many stimulating discussions. Financial support by Deutsche Forschungsgemeinschaft and Fonds der Chemie is gratefully acknowledged. P.G. thanks the Studienstiftung des Deutschen Volkes for a fellowship.

References

[1] A.-D. Gorse and M. Pesquer, J. Phys. Chem. 99 (1995) 4039.
[2] E. Lippert, W. Lüder, F. Moll, W. Nägele, H. Boos, H. Prigge and I. Seibold-Blankenstein, Angew. Chem. 21 (1961) 695.
[3] E. Lippert, W. Lüder and H. Boos, in: A. Mangini (Ed.), Advances in Molecular Spectroscopy (Pergamon Press, New York, 1962) p. 443.
[4] K. Rotkiewicz, K.H. Grellmann and Z.R. Grabowski, Chem. Phys. Lett. 19 (1973) 315.
[5] Z.R. Grabowski, K. Rotkiewicz, A. Siemiarczuk, D.J. Cowley and W. Baumann, Nouv. J. Chim. 3 (1979) 443.
[6] W. Rettig, Angew. Chem. 98 (1986) 969.
[7] W. Rettig, in N. Mataga, T. Okada and H. Masuhara (Eds.), Dynamics and mechanisms of photoinduced electron transfer and related phenomena (Elsevier, Amsterdam, 1992) p. 57.
[8] W. Rettig, Topics Current Chem. 169 (1994) 253.
[9] E. Lippert, W. Rettig, V. Bonačić-Koutecký, F. Heisel and J.A. Miehé, Adv. Chem. Phys. 68 (1987) 1.
[10] R.J. Visser and C.A.G.O. Varma, J. Chem. Soc., Farad. Trans. 2 76 (1980) 453.
[11] P.C.M. Weisenborn, A.H. Huizer and C.A.G.O. Varma, Chem. Phys. Lett. 133 (1989) 437.
[12] U. Leinhos, W. Kühnle and K.A. Zachariasse, J. Phys. Chem. 95 (1991) 2013.
[13] W. Schuddeboom, S.A. Jonker, J.M. Warman, U. Leinhos, W. Kühnle and K.A. Zachariasse, J. Phys. Chem. 96 (1992) 10809.
[14] K.A. Zachariasse, Th. von der Haar, A. Hebecker, U. Leinhos and W. Kühnle, Pure Appl. Chem. 65 (1993) 1745.
[15] K.A. Zachariasse, Th. von der Haar, U. Leinhos and W. Kühnle, J. Inf. Rec. Mats. 21 (1994) 501.
[16] Th. von der Haar, A. Hebecker, Yu. Il'ichev, W. Kühnle and K.A. Zachariasse, in: Proc. of the Conf. on Fast Elementary Processes in Chemical and Biological Systems, Lille, France, 1995.
[17] Th. von der Haar, A. Hebecker, Yu. Il'ichev, Y.-B. Jiang, W. Kühnle and K.A. Zachariasse, Recl. Trav. Chim. Pays-Bas 114 (1995) 430.
[18] O.S. Khalil, J.L. Meeks and S.P. McGlynn, Chem. Phys. Lett. 39 (1976) 457.
[19] W. Rettig and V. Bonačić-Koutecký, Chem. Phys. Lett. 62 (1979) 115.
[20] D.J. Cowley and A.H. Peoples, J. Chem. Soc. Chem. Comm. (1977) 352.
[21] J.P. LaFemina, C.B. Duke and A. Paton, J. Chem. Phys. 87 (1987) 2151.
[22] L. Serrano-Andres, M. Merchan, B.O. Ross and R. Lindh, J. Am. Chem. Soc. 117 (1995) 3189.
[23] A.L. Sobolewski and W. Domcke, Chem. Phys. Lett. 250 (1996) 428.
[24] J. Lipiński, H. Chojnacki, Z.R. Grabowski and K. Rotkiewicz, Chem. Phys. Lett. 70 (1980) 449.
[25] D. Majumdar, R. Sen, K. Bhattacharyya and S.P. Bhattacharyya, J. Phys. Chem. 95 (1991) 4324.
[26] T. Soujanya, G. Saroja and A. Samanta, Chem. Phys. Lett. 236 (1995) 503.
[27] S. Marguet, J.C. Mialocq, P. Millie, G. Berthier and F. Momicchioli, Chem. Phys. 160 (1992) 265.
[28] A.-D. Gorse and M. Pesquer, J. Mol. Struct. (Theochem.) 281 (1993) 21.
[29] A. Broo and M.C. Zerner, Theoret. Chim. Acta (Berlin) 90 (1995) 383.
[30] S. Kato and Y. Amatatsu, J. Chem. Phys. 92 (1990) 7241.
[31] S. Hayashi, K. Ando and S. Kato, J. Phys. Chem. 99 (1995) 955.
[32] J. Onsager, J. Am. Chem. Soc. 58 (1936) 1486.
[33] E.G. McRae, J. Phys. Chem. 61 (1957) 562.
[34] M.C. Zerner, ZINDO Program package, University of Florida, Gainesville.
[35] T. Fonseca, H.J. Kim and J.T. Hynes, J. Photochem. Photobiol. A: Chem. 82 (1994) 67.
[36] T. Fonseca, H.J. Kim and J.T. Hynes, J. Mol. Liq. 60 (1994) 161.
[37] H.J. Kim and J.T. Hynes, J. Photochem. Photobiol. A: Chem. in press.
[38] A. Polimeno, A. Barbon, P.L. Nordio and W. Rettig, J. Phys. Chem. 98 (1994) 12158.
[39] S. Miertuš and J. Tomasi, Chem. Phys. 65 (1982) 239.
[40] R. Bonaccorsi, R. Cimiraglia and J. Tomasi, J. Comput. Chem. 4 (1983) 567.
[41] M.A. Aguilar, F.J. Olivares del Valle and J. Tomasi, J. Chem. Phys. 98 (1993) 7375.
[42] J. Tomasi and M. Persico, Chem. Rev. 94 (1994) 2027.
[43] T. Clark, G. Rauhut, A. Alex and J. Chandrasekhar, Vamp 5.5 (Oxford Molecular, Oxford, 1994).
[44] G. Rauhut, T. Clark and T. Steinke, J. Am. Chem. Soc. 115 (1993) 9174.
[45] M.J.S. Dewar, E.G. Zoebisch, E.F. Healy and J.J.P. Stewart, J. Am. Chem. Soc. 107 (1985) 3902.
[46] G. Rauhut and T. Clark, J. Comput. Chem. 14 (1993) 503.
[47] M. Born, Z. Phys. 1 (1920) 45.
[48] J.G. Kirkwood, J. Chem. Phys. 7 (1939) 911.
[49] D. Rinaldi and J.-L. Rivail, Theoret. Chim. Acta (Berlin) 32 (1974) 243.
[50] R.A. Marcus, J. Chem. Phys. 24 (1956) 979.
[51] H.J. Kim and J.T. Hynes, J. Chem. Phys. 93 (1990) 5194.
[52] H.J. Kim and J.T. Hynes, J. Chem. Phys. 93 (1990) 5211.
[53] A. Heine, R. Herbst-Irmer, D. Stalke, W. Kühnle and K.A. Zachariasse, Acta Cryst. Sect. B: Struct. Sci. 50 (1994) 363.
[54] G.B. Jameson, B.M. Sheikh-Ali and R.G. Weiss, Acta Cryst. Sect. B: Struct. Sci. 50 (1994) 703.
[55] W. Rettig and R. Gleiter, J. Phys. Chem. 89 (1985) 4676.
[56] J.P. LaFemina, C.B. Duke and A. Paton, J. Chem. Phys. 89 (1988) 2668.
[57] J.P. LaFemina, C.B. Duke and W. Rettig, Chem. Phys. 147 (1990) 343.
[58] O. Kajimoto, H. Yokoyama, Y. Ooshima and Y. Endo, Chem. Phys. Lett. 179 (1991) 455.
[59] P. Suppan, J. Luminescence 33 (1985) 29.
[60] J.R. Platt, J. Chem. Phys. 17 (1949) 484.
[61] J.M. Hicks, M.T. Vandersall, Z. Babarogic and K.B. Eisenthal, Chem. Phys. Lett. 116 (1985) 18.
[62] F. Heisel and J.A. Miehé, Chem. Phys. 98 (1985) 233.
[63] D. Braun and W. Rettig, Chem. Phys. 180 (1994) 231.
[64] W. Liptay, Z. Naturforsch. 20a (1965) 1441.
[65] P. Gedeck, PhD thesis, Universität Erlangen-Nürnberg 1996.
[66] P. Gedeck and S. Schneider, in preparation, 1997.
[67] G. Rothenberger, D.K. Negus and R.M. Hochstrasser, J. Chem. Phys. 79 (1983) 5369.
[68] R.W. Schoenlein, L.A. Peteanu, Q. Wang, R.A. Mathies and C.V. Shank, J. Phys. Chem. 97 (1993) 12 087.